Journal of Magnetism and Magnetic Materials 624 (2025) 172992

Contents lists available at ScienceDirect

Journal of Magnetism and Magnetic Materials

journal homepage: www.elsevier.com/locate/jmmm

Research article

Magnetic properties of $(Mo_{2/3}Dy_{1/3})_2AlC$ arc melted polycrystalline samples

Binod K. Rai [a,*], Christopher A. Mizzi [b], Alex Bretaña [a], Logan Breton [a], Catherine Housley [a], Destiny Ivy [c], Joshua Abbott [c], Boris Maiorov [b], Bhoj R. Gautam [c], Matthias Frontzek [d], Ram C. Rai [e], Stuart Calder [d]

[a] Savannah River National Laboratory, Aiken, SC, 29808, USA
[b] Los Alamos National Laboratory, Los Alamos, NM 87545, USA
[c] Department of Chemistry, Physics and Materials Science, Fayetteville State University, Fayetteville, NC 28301, USA
[d] Neutron Scattering Division, Oak Ridge National Laboratory, Oak Ridge, TN 37831, USA
[e] Department of Physics, SUNY Buffalo State, Buffalo, NY 14222, USA

ARTICLE INFO

Keywords:
Rare earth i-MAX phase
Neutron diffraction
Arc melter
Antiferromagnetic ordering
Polycrystalline
Magnetic susceptibility

ABSTRACT

This study investigates the structural and magnetic properties of arc-melted $(Mo_{2/3}Dy_{1/3})_2AlC$ polycrystalline samples, a member of the *i*-MAX phase family. Temperature-dependent magnetization and specific heat measurements confirm the low-temperature antiferromagnetic transitions around 14 K and 17 K. Neutron diffraction data collected at 4 K reveal the emergence of magnetic Bragg peaks that are not allowed in the paramagnetic space group $C2/c$, further confirming the presence of antiferromagnetic ordering. The detection of a secondary phase, $DyAl_2$, is complicated by overlapping Bragg peaks with the monoclinic phase of $(Mo_{2/3}Dy_{1/3})_2AlC$ in powder XRD patterns. However, magnetization and neutron diffraction data suggest the presence of $DyAl_2$, evidenced by a ferromagnetic phase transition around 62 K.

1. Introduction

Intermetallic compounds of rare-earth elements are distinguished by their diverse compositions and crystal structures, which give rise to intriguing electronic and magnetic properties. These properties are primarily influenced by competing interactions, such as the Ruderman–Kittel–Kasuya–Yosida interactions promoting long-range magnetic order, and crystal electric-field effects (CEFs) that modify the degeneracy of the Hund's rule ground-state multiplet. A significant development in this field involves incorporating rare earth elements into $M_{n+1}AX_n$ (MAX) phases, where M denotes an early transition metal, A typically belongs to group 13 or 14, and X is carbon and/or nitrogen. The introduction of lanthanide elements had led to the creation of atomically layered *i*-MAX phases with a generic formula of $(M^1_{2/3}M^2_{1/3})_2AlC$, where transition metal elements such as Mo atoms occupy M^1 positions and form a honeycomb lattice, and the rare earth ions occupy M^2 positions and form a triangular lattice [1]. The M^1 and M^2 positions are in a 2:1 ratio and can exhibit chemical ordering in-plane (*i*-MAX) [2].

MAX phases are characterized by their unique combination of ceramic and metallic properties, drawing extensive interest from researchers due to their excellent electrical and thermal conductivities, remarkable damage tolerance, light weight, and durability at high temperatures [2–4]. There is also growing research interest in their potential magnetic and superconducting properties [3,5]. These phases serve as precursors to 2D MXenes, which are produced by etching the *A* group, such as aluminum (Al), from the MAX phase, resulting in the 2D MXene [6,7]. The introduction of non-magnetic elements Y and Sc in $(Mo_{2/3}Sc_{1/3})_2AlC$ and $(Mo_{2/3}Y_{1/3})_2AlC$, the first identified member of *i*-MAX family, has expanded the functionalities of MAX materials by allowing the synthesis of $Mo_{1.33}C$ 2D MXene structures through the removal of Al and M^2 elements [8,9]. These *i*-MXene materials have demonstrated a high volumetric capacitance of approximately ≈ 1150 Fcm^{-3} [8] and 431 F/g, highlighting the potential of new *i*-MAX and *i*-MXene materials for various applications, including as promising catalysts, supercapacitors, spintronics and batteries [4,8–12].

Investigating the complex magnetism in *i*-MAX and *i*-MXene phases presents intriguing research opportunities. For instance, in the compound $(Mo_{2/3}Sc_{1/3})_2AlC$, scandium (Sc) does not contribute to magnetism; however, incorporating rare earth element RE that exhibits magnetic moments into these phases could provide a platform to explore novel magnetic behaviors and quantum phenomena. The various magnetic interactions and CEFs offered by these rare earth elements, combined with their specific lattice arrangements, often lead to unique magnetic properties. These properties include complex and

* Corresponding author.
E-mail address: binod.rai@srnl.doe.gov (B.K. Rai).

https://doi.org/10.1016/j.jmmm.2025.172992
Received 26 January 2025; Received in revised form 28 February 2025; Accepted 19 March 2025
Available online 28 March 2025

frustrated magnetism, quantum spin liquids, quantum spin ice, topological spin textures, and metamagnetism [13–25]. Compounds such as $(Mo_{2/3}RE_{1/3})_2AlC$, where RE represents a rare earth element such as Dy that has unpaired spins, could offer unique magnetic behaviors. These compounds consist of triangular layers of magnetic rare earth ions separated by kagome-*like* layers of aluminum. The quasi-2D arrangement fosters complex magnetic properties, as demonstrated in $(Mo_{2/3}RE_{1/3})_2AlC$ [1,26], where the interaction between layers of RE, Al, and C results in magnetic frustration and complex exchange interactions. The synthesis of high-quality samples is critical for understanding the complex magnetism associated with these *i*-MAX compounds. However, achieving high-quality samples seems challenging. For instance, $(Mo_{2/3}RE_{1/3})_2AlC$ samples were synthesized by sintering at temperatures up to 1500 °C in an argon gas environment often contain impurity phases, including RE_2O_3, Mo_2C, Mo_3Al_2C, $REAlO_3$, $REAl_3C_3$, etc.[1,9]. Moreover, some rare earth *i*-MAX phases were recently reported in single crystal form [26]. For example, $(Mo_{2/3}Dy_{1/3})_2AlC$ was synthesized using induction melting at 1800 °C. However, during high-temperature induction melting, a portion of the crucible dissolves into the melt, complicating the control of stoichiometry, particularly the carbon concentration.

In this study, we synthesized polycrystalline samples of $(Mo_{2/3}Dy_{1/3})_2AlC$ using the arc melting technique in an argon gas environment. Magnetization and specific heat measurements, complemented by zero-field neutron diffraction experiments, were conducted on the arc-melted $(Mo_{2/3}Dy_{1/3})_2AlC$ samples. The physical property measurements revealed two low-temperature magnetic phase transitions, consistent with the previous reports, and an anomaly around 62.9 K, potentially arising from the $DyAl_2$ impurity phase. Powder neutron diffraction data at low-temperature (T = 4 K) revealed the emergence of scattering at reflections distinct from the crystallographic space group, aligning with previously reported antiferromagnetic phases [1, 26].

2. Methods

Polycrystalline samples of $(Mo_{2/3}Dy_{1/3})_2AlC$ were synthesized by arc-melting stoichiometric quantities of Mo (99.95%), Dy (Ames National Laboratory), Al (99.9999%), and C (99.9999%) on a water-cooled copper hearth. The ingot was flipped and remelted multiple times to ensure homogeneity. Then, the ingots were annealed for 10 days at 800 °C in a sealed quartz tube under argon. Room temperature powder X-ray diffraction data for the ground material were collected using a Rigaku SmartLab diffractometer equipped with monochromated Cu $K_{\alpha 1}$ radiation. The X-ray diffraction data were analyzed using the FullProf Suite with the Le Bail fitting method. The magnetization of polycrystalline $(Mo_{2/3}Dy_{1/3})_2AlC$ samples was measured using a Vibrating Sample Magnetometer (VSM) in a 14T Quantum Design Physical Property Measurement System (PPMS). Specific heat measurements were conducted using a 9T Quantum Design PPMS.

Neutron powder diffraction was performed on the HB-2A powder diffractometer at High Flux Isotope Reactor (HFIR), ORNL, using ground powder from the annealed ingots [27]. The powder sample was placed in Al foil and wrapped around the inner walls of a 15 mm Al can. This geometry and sample preparation method reduced the neutron absorption to allow for an increased signal; however this annular geometry makes detailed refinements of the data more challenging. Measurements were collected with a wavelength of 2.41 Å selected from the Ge (113) reflection of the monochromator. Diffraction patterns were measured at temperatures of 4 K, 40 K and 80 K. To follow the temperature dependence of certain reflections a single detector was placed at the appropriate two-theta position and the temperature varied.

3. Results

3.1. Synthesis and structural characterization

The synthesis of MAX phases typically demands high-temperature and or vacuum or inert atmospheric conditions due to the stringent requirements for crystal growth. These include the high melting points of the starting materials and their susceptibility to oxidation in the absence of a vacuum or inert gas environment. In the case of the *i*-MAX phase, the synthesis is further complicated by the need to navigate an unknown fourth-dimensional phase diagram and the purity of rare earth elements. These challenges limit the applicability of a few crystal growth methods such as sintering, induction melting, or arc melting. For instance, the milling/sintering approach often results in oxide and carbide impurities [1,9,28], while induction melting can lead to contamination from graphite crucibles [26]. In our study, we synthesized $(Mo_{2/3}Dy_{1/3})_2AlC$ using high-purity elements, including rare earth metals sourced from Ames Lab. The synthesis was carried out in an arc melter, with the sample chamber purged 4–5 times with argon to ensure a clean environment. Additionally, the sample was flipped 3–4 times during the process to achieve homogeneity.

The room temperature powder XRD data were collected on a Bruker D8 powder diffractometer with a Cu source ($\lambda_{k\alpha}$ = 1.5406 Å), as shown in Fig. 1. The $(Mo_{2/3}Dy_{1/3})_2AlC$ powder diffraction pattern is well indexed by the mononclinic structure *i*-MAX phase with the space group $C2/c$, using Le Bail fitting with the goodness of fit χ^2 = 6.4 (see Fig. 1(a)). The refined lattice parameters in space group $C2/c$ are a = 9.371(9)Å, b = 5.503(3)Å, c = 14.13(1)Å and β = 104.8(1)°, which are in consistent with the literature [1,26]. Based on the magnetization data discussed below, $(Mo_{2/3}Dy_{1/3})_2AlC$ appears to contain a secondary phase of $DyAl_2$, whose nuclear Bragg peaks overlap with the main phase such as $2\theta \approx$ 19.6, 32.5, and 38°. $DyAl_2$ crystallizes in a space group $Fd\bar{3}m$ with the lattice parameters $a = b = c$ = 7.8424 Å and $\alpha = \beta = \gamma$ = 90°. The powder diffraction pattern indexed by the monoclinic structure *i*-MAX phase and the cubic $DyAl_2$ phase, using Le Bail fitting with the goodness of fit χ^2 = 5.3 is shown Fig. 1(b). Underfitting of the $00l$ reflections, noticeable around 12, 26, and 36 degrees among other angles, could be attributed to the intrinsic properties of layered MAX materials.

The crystal structure of $(Mo_{2/3}Dy_{1/3})_2AlC$ is composed of two building blocks, A and B, which are stacked down the c-axis separated by layers of aluminum atoms (Fig. 2(a)). Block A and B are both constructed of carbon-centered Mo_3Dy_2C octahedra which edge-share along the $a-b$ axis (Fig. 2(a)). There are two crystallographically unique Mo_3Dy_2C octahedra dependent on the equatorial or axial positions of Mo or Dy within the octahedra (Fig. 2(b,c)). The building blocks are stacked in an ABAB sequence with the B block rotated +60° relative to A [5,29].

The *i*-MAX structure type is characterized by the in-plane chemical ordering of the metal atoms as well as a Kagome-*like* orientation of the Al atom plane. The metal atoms within the plane are "buckled" due to the atomic size difference between M^1 and M^2, where M^2 extends away from M^1 and towards the Al atom plane which renders the Al Kagome-*like* lattice. This structure contrasts with the general formula $M_{n+1}AC_n$, where all M atoms lie in the same plane, forming a honeycomb lattice with another M atom occupying the hexagonal center of the honeycomb [2]. The *i*-MAX structure of $(Mo_{2/3}Dy_{1/3})_2AlC$ is comprised of laminated atomic planes of Al, C, and Mo/Dy, which are stacked down the c-axis in the order Al-Dy/Mo-C-Mo/Dy-Al. Fig. 2(a) illustrates the characteristic "buckled" nature of the Dy/Mo plane as the atomic size difference between Mo and Dy results in the extension of Dy away from Mo. This creates individual quasi-2D sheets of both Dy and Mo atoms with Dy atoms oriented in a triangular lattice and Mo atoms in a honeycomb lattice, Fig. 2(d–e). The extension of the Dy atoms towards the Al atom layer results in the characteristic Kagome-*like* lattice of the Al atoms, Fig. 2(f). The C atom plane is sandwiched between two Dy/Mo atom planes oriented in a triangular lattice, Fig. 2(g).

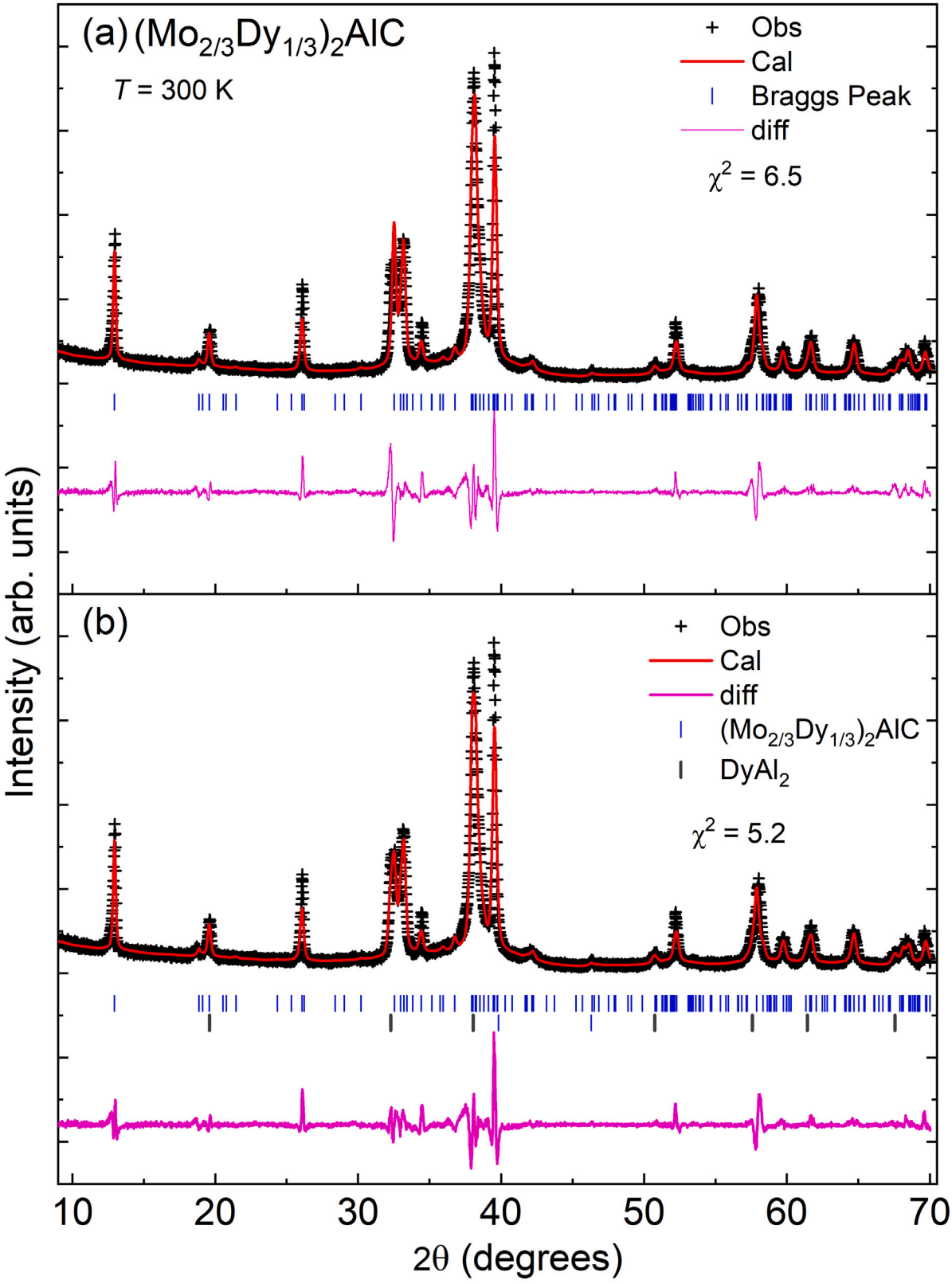

Fig. 1. Room-temperature powder diffraction pattern of $(Dy_{1/3}Mo_{2/3})_2AlC$ for a pulverized crystal (symbol) together with the Le Bail fitting (red line) and Bragg positions (vertical lines). Refinement of $(Dy_{1/3}Mo_{2/3})_2AlC$ pattern (a) without $DyAl_2$ (b) with $DyAl_2$ phase.

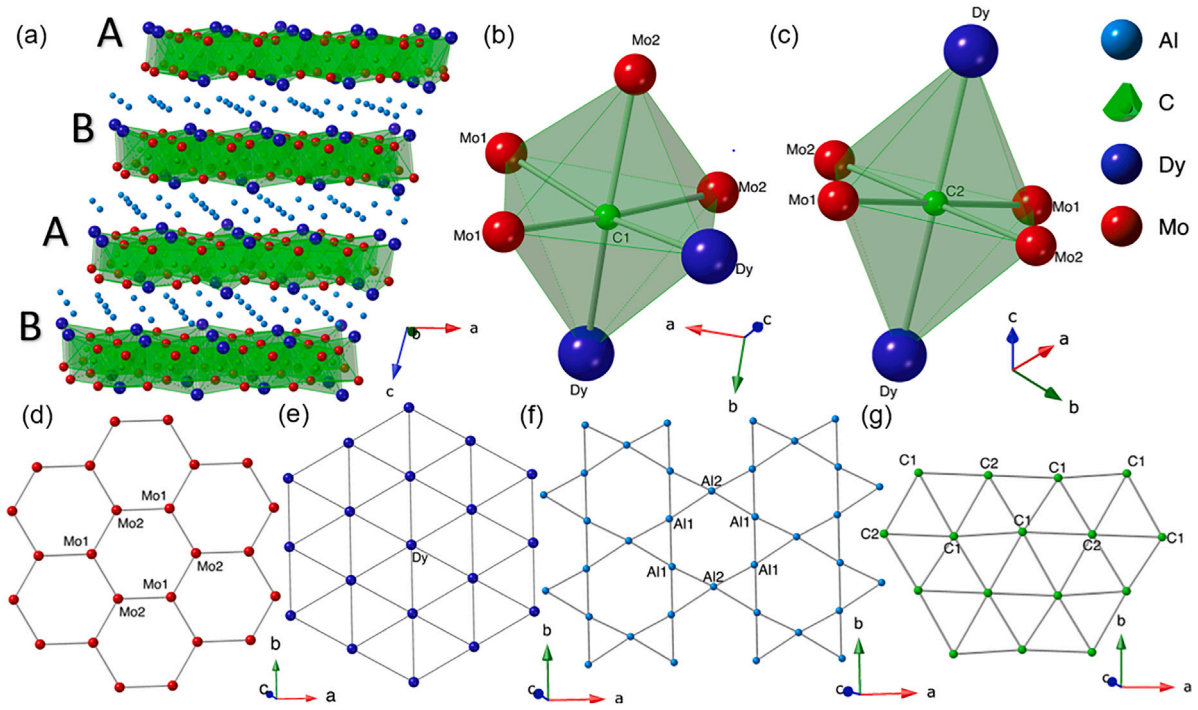

Fig. 2. A schematic of the crystal structure of $(Dy_{1/3}Mo_{2/3})_2AlC$ illustrating the (a) full crystal structure, (b,c) carbon-centered Mo_3Dy_2C octahedra (d) Mo honeycomb lattice, (e) *RE* triangular lattice, (f) Al Kagome-*like* lattice, and (g) carbon triangular lattice.

3.2. Magnetic properties

The magnetization data for arc melted polycrystalline samples of $(Mo_{2/3}Dy_{1/3})_2AlC$ is illustrated in Fig. 3. Temperature-dependent magnetization measurements (M/H *vs.* T) reveal multiple anomalies below 100 K, including an upturn in magnetization upon cooling, as shown in Fig. 3(a). This upturn in M/H *vs.* T around 60 K, previously noted in studies of $(Mo_{2/3}Dy_{1/3})_2AlC$ single crystals, wa attributed to crystal electric field effects [26]. Notably, the upturn observed in our samples appears more pronounced than in previously published reports [26]. The inset of Fig. 3(a) shows the derivative of M/H *vs.* T data, showing a dip around 62.9 K. This transition temperature coincides with the ferromagnetic phase transition of $DyAl_2$[30]. Barbier *et al.* [26] highlighted this complexity by analyzing magnetization along all three crystallographic axes of the monoclinic structure of a $(Mo_{2/3}Dy_{1/3})_2AlC$ single crystal, where the M/H *vs.* T single crystal data along *a*-axis is similar to our polycrystalline data. The high-temperature magnetization H/M *vs.* T (150-300 K) displays Curie–Weiss behavior, as shown in Fig. 3(b). The effective moment per Dy element, estimated from the Curie–Weiss fit of the inverse magnetic susceptibility ($1/\chi = H/M$), is $\mu_{eff} = 10.43\ \mu_B$/Dy and the Weiss temperature $\theta_W = 21.2$ K. The effective moment of our sample is consistent with the previously published reports (10.5 μ_B/Dy) [1] and 10.6 μ_B/Dy [26].

Isothermal magnetization curves $M(H)$ of $(Mo_{2/3}Dy_{1/3})_2AlC$ for the polycrystalline sample are shown in Fig. 4(a), where data collected at 2 K display several metamagnetic transitions, mirroring findings from the single crystal study [26]. Although derived from polycrystalline samples, the $M(H)$ characteristics at 2 K resemble those observed along the crystallographic *a*-axis of the single crystalline samples. According to Barbier *et al.* [26], the magnetic easy axis is along the *a*-axis, with magnetic moments of approximately 9.3 μ_B/Dy and hard axis along the *c*-axis with 0.5 μ_B/Dy at $\mu_0 H = 5$T. The single crystal $M(H)$ data show metamagnetic transitions at 1, 4.5, and 5T along the *a*-axis, a transition at 4.5 T along the *b*-axis, and no transitions along the *c*-axis. These findings highlight highly anisotropic and the complex magnetic behavior of $(Mo_{2/3}Dy_{1/3})_2AlC$. Our polycrystalline data shows metamagnetic transitions around 1 and 4.75T (marked by arrows in Fig. 4(b)), consistent with the prior report [26], while the $M(H)$ data at 200 K show paramagnetic behavior.

Specific heat measurements ($C_p(T)$) were also performed in zero and applied magnetic fields to explore the observed phase transitions further, as shown in Fig. 5. At zero field, $C_p(T)$ of $(Mo_{2/3}Dy_{1/3})_2AlC$ exhibits anomalies at ~ 14, 17, and 62 K. The low-temperature phase transitions (T = 14 and 17 K) align with the transition temperatures (T_N) reported in previous studies [1,26,31]. The inset of Fig. 5 displays the $C_p(T)$ data under applied fields, which demonstrate an enhancement of specific heat with up to 2T magnetic fields, followed by suppression at the higher applied magnetic field. This behavior is consistent with earlier reports [26,31]. Additionally, the $C_p(T)$ data exhibit a complex response for low-temperature phase transitions under applied fields, and the anomaly is still not fully suppressed under an applied field of 9T, also consistent with earlier reports [26,31].

3.3. Neutron diffraction

We have collected low-temperature powder neutron diffraction data at $T = 4$ K, as shown in Fig. 6, showing several additional Bragg peaks compared with diffraction data at 40 K, indicating antiferromagnetic ordering at low temperatures. The peaks for an antiferromagnetic phase seem consistent with previous neutron diffraction studies. These studies report a commensurate structure characterized by a propagation vector $\vec{k}$ = (0, 1/2, 0) observed below T_{N2} (down to 2 K) [26,31]. Measurement of the temperature dependence of the magnetic Bragg peak at Q = 0.73 Å^{-1} is presented in Fig. 6(b). This shows a marked increase in intensity as the temperature decreases. Notably, the increase in intensity at this Q position below 20 K corresponds to the antiferromagnetic transitions.

We also collected neutron diffraction data at temperatures of 40 K and 80 K, the latter within the paramagnetic range, as depicted in Fig. 7. At 40 K, the Bragg peaks correspond solely to the crystal lattice reflection positions. However, an enhancement of Bragg peaks at Q = 1.39 and 2.28 Å^{-1} relative to the nuclear reflections observed at 80 K is evident. This enhancement coincides with a ferromagnetic nature associated with the phase transition at $T = 62.9$ K of $DyAl_2$ (see Fig.

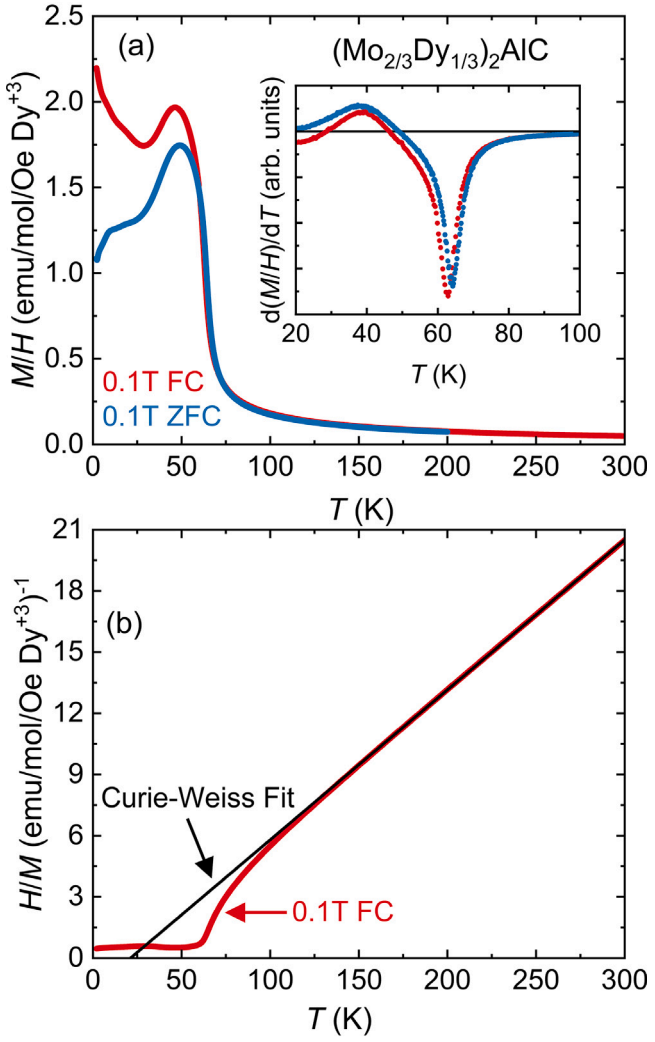

Fig. 3. (a) The temperature-dependent magnetization M/H *vs.* T data of $(Mo_{2/3}Dy_{1/3})_2AlC$ at an applied magnetic field $\mu_0 H = 0.1$ T. Inset: the derivatives of the temperature-dependent magnetization $d(M/H)/dT$ data. (b) The inverse magnetization $(1/\chi = H/M)$ at the applied magnetic field $\mu_0 H = 0.1$ T. The black line is the Curie Weiss model fitted between 150 and 300 K.

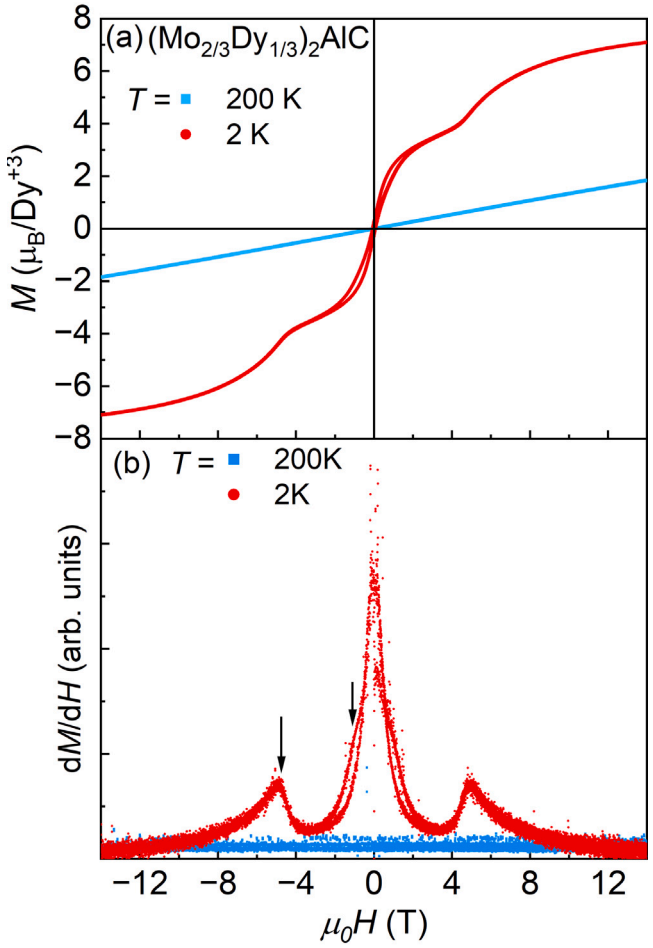

Fig. 4. (a) The isothermal magnetization M *vs.* H data of $(Mo_{2/3}Dy_{1/3})_2AlC$ at 2 K and 200 K. (b) The derivatives of the isothermal magnetization dM/dH of $(Mo_{2/3}Dy_{1/3})_2AlC$. Arrows indicate the metamagnetic phase transitions field positions of $(Mo_{2/3}Dy_{1/3})_2AlC$.

7) and is consistent with the spontaneous magnetization data (see Fig. 3(a)). Note: $Q = 2.66$ Å^{-1} peak associated with the main phase and $DyAl_2$ also coincide with the Al can peak and is therefore excluded from the comparison of enhanced Bragg peaks.

3.4. Discussion and summary

Both MAX and MXene materials are attracting significant attention due to their exceptional electrical and thermal conductivities, damage tolerance, durability at high temperatures, and intriguing magnetic and electrochemical properties [2,3,3–5,32–34]. Within this family, the *i*-MAX phase $(Mo_{2/3}RE_{1/3})_2AlC$ has drawn particular interest for its unique electronic and complex magnetic properties. The quality of the samples is critical for understanding the ground state of these compounds. However, *i*-MAX polycrystalline samples seem to exhibit magnetic and or superconducting impurity phases such as RE_2O_3, Mo_2C, Mo_3Al_2C, $REAlO_3$, $REAl_3C_3$, $REAl_2$, etc [1,9,35] or suffer from off-stoichiometry carbon content in single crystal sample due to the graphite crucible melt [26]. Recently, $(Mo_{2/3}Gd_{1/3})_2AlC$ has been reported to magnetically order at 26 K, with two impurity phases identified: the ferromagnetic compound $GdAl_2$ (T_C = 170 K, ~ 0.7

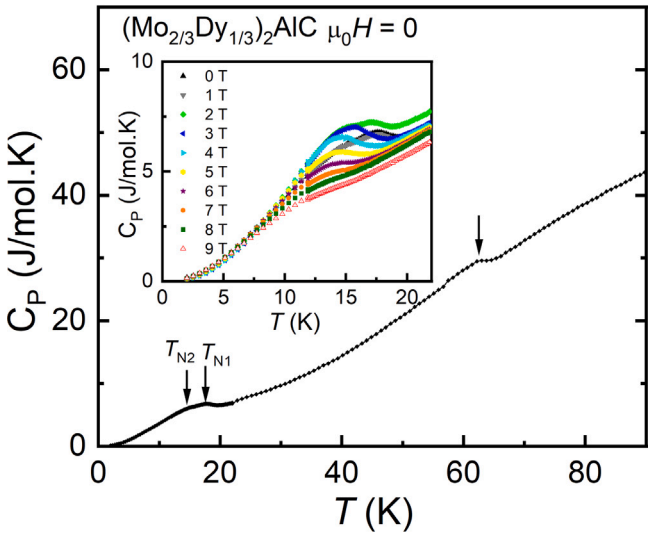

Fig. 5. Specific heat capacity C_p of $(Mo_{2/3}Dy_{1/3})_2AlC$ in zero applied field demonstrating anomalies at T_{N1} and T_{N2}. Inset: C_p of $(Mo_{2/3}Dy_{1/3})_2AlC$ under applied magnetic fields. The anomaly at ~ 62 K could arise from the secondary phase $DyAl_2$.

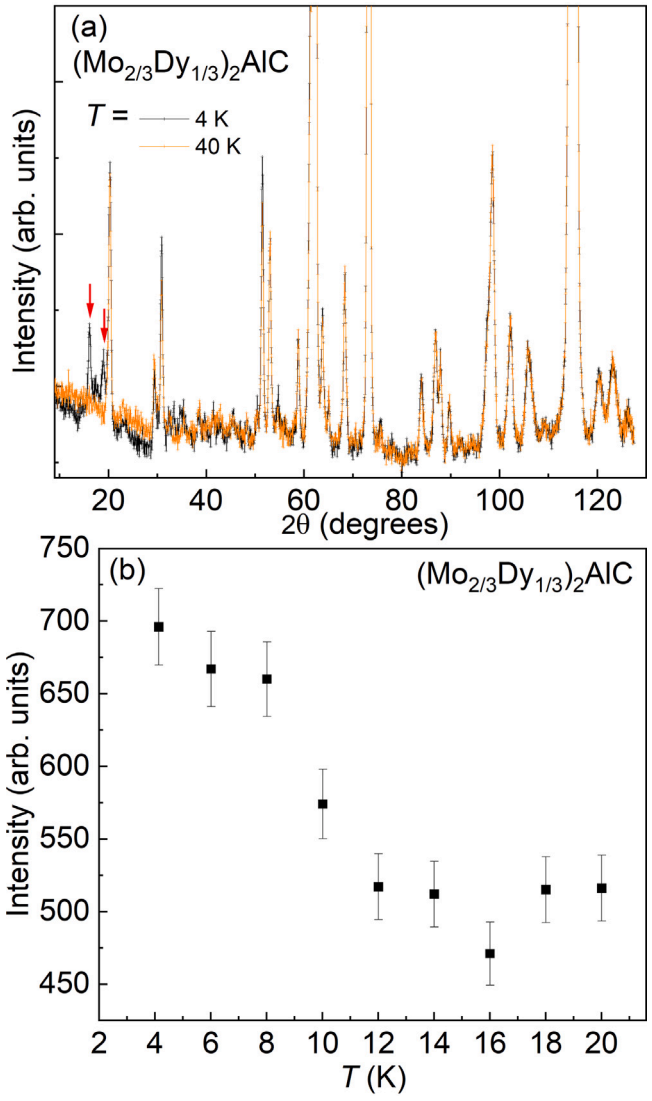

Fig. 6. (a) Neutron powder diffraction pattern of $(Mo_{2/3}Dy_{1/3})_2AlC$ at $T = 4$ K $< T_N$ and $T = 40$ K $> T_N < T_C$ shows the additional Bragg peaks at $T = 4$ K that are not allowed by the crystal structure, revealing antiferromagnetic contribution associated with the magnetization anomaly below T_N. (b) Magnetic order parameter of $(Mo_{2/3}Dy_{1/3})_2AlC$ measured at $Q = 0.73$ Å^{-1} upon warming. Error bars represent the square root of the counts.

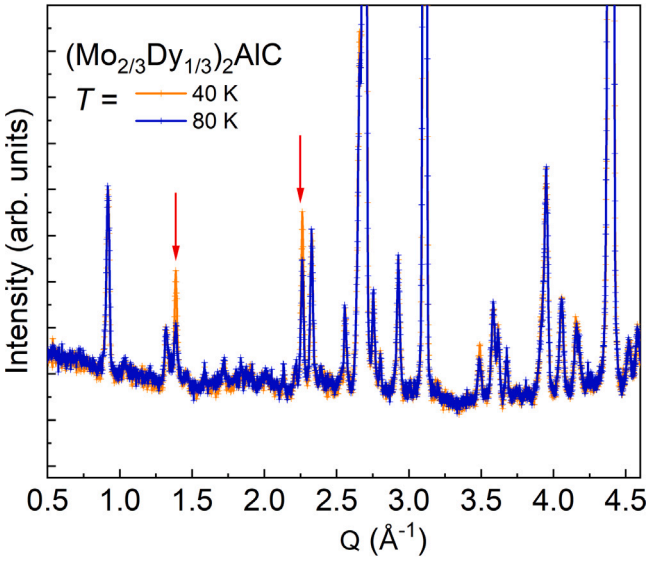

Fig. 7. Neutron powder diffraction pattern of $(Mo_{2/3}Dy_{1/3})_2AlC$ at $T = 40$ K $< T_C$ and $T = 80$ K $> T_C$ shows the enhancement of Bragg peaks at $T = 40$ K on top of nuclear Bragg peaks at $T = 80$ K. The position and enhancement of these Bragg peaks coincide with reflections of $DyAl_2$.

wt%) and the superconducting phase Mo_3Al_2C ($T_c = 9.2$ K) [35]. The cubic $REAl_2$ phase like $DyAl_2$ presents another challenge as its nuclear Bragg peaks coincide with those of the monoclinic crystal structure $(Mo_{2/3}Dy_{1/3})_2AlC$ (space group $C2/c$), making it difficult to distinguish this ferromagnetic impurity phase by the powder XRD data alone. However, due to its ferromagnetic nature, the magnetic susceptibility is dominated by the spontaneous magnetization near its magnetic transition.

This article presents a detailed investigation into the structural and magnetic characteristics of arc melted $(Mo_{2/3}Dy_{1/3})_2AlC$ polycrystalline samples. The low-temperature magnetization and specific heat data confirm low-temperature phase transitions consistent with antiferromagnetic transitions around 14 K and 17 K reported in the literature. Furthermore, additional Bragg peaks incompatible with the paramagnetic space group $C2/c$ were observed at 4 K, confirming antiferromagnetic ordering at lower temperatures. Our magnetic susceptibility data also reveal a spontaneous ferromagnetic transition at 62.9 K, perhaps attributed to the secondary phase $DyAl_2$. However, this secondary phase of $DyAl_2$ is difficult to detect using powder XRD data alone, as its Bragg peaks overlap with those of the monoclinic phase $(Mo_{2/3}Dy_{1/3})_2AlC$, complicating its detection. This work underscores the complexity of synthesizing high-purity *i*-MAX phases, which often include magnetic and superconducting impurity phases, and highlights the need for various characterization techniques to disentangle the structural and magnetic contributions in these compounds.

CRediT authorship contribution statement

Binod K. Rai: Writing – review & editing, Writing – original draft, Visualization, Validation, Supervision, Software, Resources, Project administration, Methodology, Investigation, Funding acquisition, Formal analysis, Data curation, Conceptualization. **Christopher A. Mizzi:** Writing – review & editing, Software, Methodology, Formal analysis, Data curation. **Alex Bretaña:** Writing – review & editing, Software, Methodology. **Logan Breton:** Writing – review & editing, Software. **Catherine Housley:** Writing – review & editing, Data curation. **Destiny Ivy:** Writing – review & editing, Methodology, Data curation. **Joshua Abbott:** Writing – review & editing, Software, Data curation. **Boris Maiorov:** Writing – review & editing, Software, Methodology, Formal analysis, Data curation. **Bhoj R. Gautam:** Writing – review & editing, Funding acquisition. **Matthias Frontzek:** Writing – review & editing, Formal analysis, Data curation. **Ram C. Rai:** Writing – review & editing, Software, Formal analysis, Data curation. **Stuart Calder:** Writing – review & editing, Validation, Software, Investigation, Formal analysis, Data curation.

Declaration of competing interest

The authors declare that they have no known competing financial interests or personal relationships that could have appeared to influence the work reported in this paper.

Acknowledgments

We would like to thank Gia Thinh Tran for helpful discussions. We acknowledge the U.S. Department of Energy Office of Science, Basic Energy Sciences, condensed matter physics program (award number

DE-SC0024611). This work was produced by Battelle Savannah River Alliance, LLC under Contract No. 89303321CEM000080 with the U.S. Department of Energy. Publisher acknowledges the U.S. Government license to provide public access under the DOE Public Access Plan (http://energy.gov/downloads/doe-public-access-plan). This research used resources at the High Flux Isotope Reactor, a DOE Office of Science User Facility operated by the Oak Ridge National Laboratory. The beam time was allocated to HB-2 A (POWDER) on proposal number IPTS-32938.1 and 32431.1. A portion of this work was performed at the National High Magnetic Field Laboratory, which is supported by National Science Foundation Cooperative Agreement No. DMR-2128556, the State of Florida and the U.S. Department of Energy. Research presented in this article was supported by the Laboratory Directed Research and Development program of Los Alamos National Laboratory under project number 20240225ER.

Data availability

Data will be made available on request.

References

[1] Q. Tao, J. Lu, M. Dahlqvist, A. Mockute, S. Calder, A. Petruhins, R. Meshkian, O. Rivin, D. Potashnikov, E.N. Caspi, et al., Atomically layered and ordered rare-earth i-MAX phases: a new class of magnetic quaternary compounds, Chem. Mater. 31 (7) (2019) 2476–2485.

[2] B. Ahmed, A.E. Ghazaly, J. Rosen, i-MXenes for energy storage and catalysis, Adv. Funct. Mater. 30 (47) (2020) 2000894.

[3] P. Eklund, M. Beckers, U. Jansson, H. Högberg, L. Hultman, The $M_{n+1}AX_n$ phases: Materials science and thin-film processing, Thin Solid Films 518 (8) (2010) 1851–1878.

[4] A. Mockute, Q. Tao, M. Dahlqvist, J. Lu, S. Calder, E. Caspi, L. Hultman, J. Rosén, Materials synthesis, neutron powder diffraction, and first-principles calculations of $(Mo_xSc_{1-x})_2AlC$ i-MAX phase used as parent material for MXene derivation, Phys. Rev. Mater. 3 (11) (2019) 113607.

[5] A. Petruhins, M. Dahlqvist, J. Lu, L. Hultman, J. Rosen, Theoretical prediction and experimental verification of the chemically ordered atomic-laminate i-MAX phases $(Cr_2/3Sc_{1/3})_2GaC$ and $(Mn_{2/3}Sc_{1/3})_2GaC$, Cryst. Growth & Des. 20 (1) (2019) 55–61.

[6] M. Ghidiu, M.R. Lukatskaya, M.-Q. Zhao, Y. Gogotsi, M.W. Barsoum, Conductive two-dimensional titanium carbide 'clay' with high volumetric capacitance, Nature 516 (2014) 78–81.

[7] J. Halim, M.R. Lukatskaya, K.M. Cook, J. Lu, C.R. Smith, L.-Å. Näslund, S.J. May, L. Hultman, Y. Gogotsi, P. Eklund, et al., Transparent conductive two-dimensional titanium carbide epitaxial thin films, Chem. Mater. 26 (7) (2014) 2374–2381.

[8] Q. Tao, M. Dahlqvist, J. Lu, S. Kota, R. Meshkian, J. Halim, J. Palisaitis, L. Hultman, M.W. Barsoum, P.O. Persson, et al., Two-dimensional $Mo_{1.33}C$ MXene with divacancy ordering prepared from parent 3D laminate with in-plane chemical ordering, Nat. Commun. 8 (1) (2017) 14949.

[9] J. Yang, G. Yao, S. Sun, Z. Chen, S. Yuan, K. Wu, X. Fu, Q. Wang, W. Cui, Structural, magnetic properties of in-plane chemically ordered $(Mo_2/3R_{1/3})_2AlC$ (R=Gd, Tb, Dy, Ho, Er and Y) MAX phase and enhanced capacitance of $Mo_{1.33}C$ MXene derivatives, Carbon 179 (2021) 104–110.

[10] I. Persson, A. El Ghazaly, Q. Tao, J. Halim, S. Kota, V. Darakchieva, J. Palisaitis, M.W. Barsoum, J. Rosen, P.O. Persson, Tailoring structure, composition, and energy storage properties of MXenes from selective etching of in-plane, chemically ordered MAX phases, Small 14 (17) (2018) 1703676.

[11] Y. He, W. Zhou, J. Xu, Rare earth-based nanomaterials for supercapacitors: Preparation, structure engineering and application, ChemSusChem 15 (12) (2022) e202200469.

[12] J. Abbott, V. Morris, M. Adhikari, S. Balabhadra, A. Bretaña, B. Rai, D. Autrey, B. Gautam, Structural and Morphological Characteristics of Rare Earth Element-based MAX Phase and MXene, Oxford University Press, US, 2024.

[13] A. Hallas, C. Huang, B.K. Rai, A. Weiland, G.T. McCandless, J.Y. Chan, J. Beare, G. Luke, E. Morosan, Complex transport and magnetism in inhomogeneous mixed valence $Ce_3Ir_4Ge_13$, Phys. Rev. Mater. 3 (11) (2019) 114407.

[14] D. Yahne, D. Pereira, L. Jaubert, L. Sanjeewa, M. Powell, J. Kolis, G. Xu, M. Enjalran, M. Gingras, K. Ross, Understanding reentrance in frustrated magnets: the case of the $Er_2Sn_2O_7$ pyrochlore, Phys. Rev. Lett. 127 (27) (2021) 277206.

[15] C.M. Pasco, B.K. Rai, M. Frontzek, G. Sala, M.B. Stone, B.C. Chakoumakos, V.O. Garlea, A.D. Christianson, A.F. May, Anisotropic magnetism of the Shastry-Sutherland lattice material $BaNd_2PtO_5$, Phys. Rev. Mater. 7 (7) (2023) 074407.

[16] B.K. Rai, B. Maiorov, K. Gofryk, P. O'Rourke, C. Housley, H. Ajo, A. Sawon, A.K. Pathak, N. Poudel, Q. Zhang, et al., Structure and properties of $NdCuGa_3$ single crystals, J. Magn. Magn. Mater. 589 (2024) 171515.

[17] J.A. Paddison, B.K. Rai, A.F. May, S. Calder, M.B. Stone, M.D. Frontzek, A.D. Christianson, Magnetic interactions of the centrosymmetric skyrmion material Gd_2PdSi_3, Phys. Rev. Lett. 129 (13) (2022) 137202.

[18] S. Calder, Z. Zhao, M. Upton, J.-Q. Yan, Local site behavior of the 5d and 4f ions in the frustrated pyrochlore $Ho_2Os_2O_7$, Phys. Rev. B 109 (5) (2024) 054408.

[19] B.K. Rai, P. O'Rourke, U.N. Roy, Review on crystal structures and magnetic properties of RTX_3 materials, J. Phys.: Condens. Matter. 34 (27) (2022) 273002.

[20] K.A. Ross, L. Savary, B.D. Gaulin, L. Balents, Quantum excitations in quantum spin ice, Phys. Rev. X 1 (2) (2011) 021002.

[21] J.-J. Wen, S. Koohpayeh, K. Ross, B. Trump, T. McQueen, K. Kimura, S. Nakatsuji, Y. Qiu, D. Pajerowski, J. Copley, et al., Disordered route to the coulomb quantum spin liquid: Random transverse fields on spin ice in $Pr_2Zr_2O_7$, Phys. Rev. Lett. 118 (10) (2017) 107206.

[22] G. Sala, M.B. Stone, B.K. Rai, A.F. May, P. Laurell, V.O. Garlea, N.P. Butch, M.D. Lumsden, G. Ehlers, G. Pokharel, et al., Van Hove singularity in the magnon spectrum of the antiferromagnetic quantum honeycomb lattice, Nat. Commun. 12 (1) (2021) 171.

[23] B.K. Rai, G. Pokharel, H.S. Arachchige, S.-H. Do, Q. Zhang, M. Matsuda, M. Frontzek, G. Sala, V.O. Garlea, A.D. Christianson, et al., Complex magnetic phases in the polar tetragonal intermetallic $NdCoGe_3$, Phys. Rev. B 103 (1) (2021) 014426.

[24] B.R. Ortiz, P.M. Sarte, G. Pokharel, M.J. Knudtson, S.J. Gomez Alvarado, A.F. May, S. Calder, L. Mangin-Thro, A.R. Wildes, H. Zhou, et al., Revisiting spin ice physics in the ferromagnetic Ising pyrochlore $Pr_2Sn_2O_7$, Phys. Rev. B 109 (13) (2024) 134420.

[25] B.K. Rai, S. Chikara, X. Ding, I.W. Oswald, R. Schönemann, V. Loganathan, A. Hallas, H. Cao, M. Stavinoha, T. Chen, et al., Anomalous metamagnetism in the low carrier density kondo lattice $YbRh_3Si_7$, Phys. Rev. X 8 (4) (2018) 041047.

[26] M. Barbier, F. Wilhelm, C.V. Colin, C. Opagiste, E. Lhotel, D. Pinek, Y. Kim, D. Braithwaite, E. Ressouche, P. Ohresser, et al., Magnetic properties of the $(Mo_2/3R_{1/3})_2AlC$ (R=Ho, Dy) i-MAX phases studied by X-ray magnetic circular dichroism and neutron diffraction, Phys. Rev. B 105 (17) (2022) 174421.

[27] S. Calder, K. An, R. Boehler, C.R. Dela Cruz, M.D. Frontzek, M. Guthrie, B. Haberl, A. Huq, S.A. Kimber, J. Liu, et al., A suite-level review of the neutron powder diffraction instruments at Oak Ridge National Laboratory, Rev. Sci. Instrum. 89 (9) (2018).

[28] J. Lu, A. Thore, R. Meshkian, Q. Tao, L. Hultman, J. Rosén, Theoretical and experimental exploration of a novel in-plane chemically ordered $(Cr_2/3M_{1/3})_2AlC$ $i-MAX$ phase with M=Sc and Y, Cryst. Growth & Des. 17 (11) (2017) 5704–5711.

[29] A. Champagne, O. Chaix-Pluchery, T. Ouisse, D. Pinek, I. Gélard, L. Jouffret, M. Barbier, F. Wilhelm, Q. Tao, J. Lu, et al., First-order Raman scattering of rare-earth containing i-MAX single crystals $(Mo_2/3RE_{1/3})_2AlC$ (RE=Nd, Gd, Dy, Ho, Er), Phys. Rev. Mater. 3 (5) (2019) 053609.

[30] N. Nereson, C. Olsen, G. Arnold, Magnetic properties of $DyAl_2$ and $NdAl_2$, J. Appl. Phys. 37 (12) (1966) 4575–4580.

[31] Q. Tao, M. Barbier, A. Mockute, C. Ritter, R. Salikhov, U. Wiedwald, S. Calder, C. Opagiste, R.-M. Galera, M. Farle, et al., Magnetic phase diagram of $(Mo_2/3RE_{1/3})_2AlC$, RE=Tb and Dy, studied by magnetization, specific heat, and neutron diffraction analysis, J. Phys.: Condens. Matter. 34 (21) (2022) 215801.

[32] Z. Lin, M. Li, J. Wang, Y. Zhou, High-temperature oxidation and hot corrosion of Cr_2AlC, Acta Mater. 55 (18) (2007) 6182–6191.

[33] G. Ying, X. He, M. Li, W. Han, F. He, S. Du, Synthesis and mechanical properties of high-purity Cr_2AlC ceramic, Mater. Sci. Eng.: A 528 (6) (2011) 2635–2640.

[34] S. Sun, Z. Ma, Z. Chen, P. Liu, Y. Song, Q. Lu, X. Fu, Q. Wang, W. Cui, The crystallographic structure and properties of novel quaternary nanolaminated rare-earth-Cr-based i-MAX phases, Acta Mater. 242 (2023) 118479.

[35] D. Yahav, A. Maniv, D. Potashnikov, A. Pesach, E.N. Caspi, A.P. Reyes, Q. Tao, J. Rosen, E. Maniv, Hidden magnetic phases in i-MAX compounds, 2024, arXiv preprint arXiv:2412.02418.